Title: Novel Role of AcylCoA:cholesterol acyltransferase 1 (ACAT1/SOAT1) in Diabetic Retinopathy

Authors: Syed Adeel H. Zaidi [1,2,3], Tahira Lemtalsi [1,2], Zhimin Xu [1,2], Mai Yamamoto [1,2], Porsche V. Sandow [7], Steven E. Brooks [2,5], R. William Caldwell [2,4], Ruth B. Caldwell [1,2,5,6,*], Modesto A. Rojas [1,2,4,*]

Affiliations:

[1] Vascular Biology Center, Medical College of Georgia, Augusta University, Augusta, GA 30912, USA

[2] Culver Vision Discovery Institute, Medical College of Georgia, Augusta University, Augusta, GA 30912, USA

[3] Department of Medicine, Medical College of Georgia, Augusta University, Augusta, GA 30912, USA

[4] Department of Pharmacology and Toxicology, Medical College of Georgia, Augusta University, Augusta, GA 30912, USA

[5] Department of Ophthalmology, Medical College of Georgia, Augusta University, Augusta, GA 30912, USA

[6] Department of Cellular Biology and Anatomy, Medical College of Georgia, Augusta University, Augusta, GA 30912, USA

[7]School of Medicine University of New Mexico, Albuquerque, NM, 87106, USA

*Address of correspondence for this article

Ruth B. Caldwell, PhD	Modesto A. Rojas, MD
Vascular Biology Center	Vascular Biology Center
1460 Laney Walker Blvd	1460 Laney Walker Blvd
Augusta University	Augusta University
Augusta, GA 30912-2500	Augusta, GA 30912-2500
Tel: 706-721-6145	Tel: 706-721-7412
Email: rcaldwel@augusta.edu	Email: mrojas@augusta.edu

One sentence summary: Inhibiting cholesterol esterification limits retinal neurovascular injury in diabetes.

ABSTRACT

Hypercholesterolemia and excessive cholesterol ester (CE) production have been linked to chronic inflammation and vascular dysfunction during cardiovascular disease. Upregulation of AcylCoA:cholesterol acyltransferase 1 (ACAT1/SOAT1), the enzyme responsible for retinal CE formation, has been implicated in pathological retinal neovascularization. Here we determine the role of this process in diabetic retinopathy (DR). Ins2^{Akita} diabetic mice were treated with the specific ACAT1/SOAT1 inhibitor K604 (10 mg/Kg, i.p.) beginning at 10 weeks for 2 weeks or 8 months for 2 months. ACAT1/SOAT1 expression and CE formation were assayed along with oxidative stress, inflammation, vascular pathology, and neuronal function. ACAT1/SOAT1 expression was also assayed in human retinas and vitrectomy specimens. Retinas from early-stage Ins2^{Akita} mice exhibited increases in CE deposition, superoxide production, and expression of ACAT1/SOAT1, LDLR, TREM1, MCSF, and VEGF along with leukostasis, vascular leakage, acellular capillary formation, retinal ganglion cell loss, and impaired visual function. Late-stage

increases in CE, ACAT1/SOAT, oxidative stress, inflammation, and impaired visual function were also observed. These changes were significantly inhibited by K604 treatment. The protective effects were independent of changes in systemic glucose or body weight. Human retina and vitrectomy samples also showed increases in ACAT1/SOAT1 and CE, respectively. Specific inhibition of ACAT1/SOAT1 with K604 normalizes ACAT1/SOAT1 expression and CE formation and prevents increases in oxidative stress and inflammation and preserves retinal structure and function in both early and late stages of DR. These findings identify ACAT1/SOAT1 as a promising therapeutic target for both early intervention and later stage treatment of DR.

INTRODUCTION

Diabetic retinopathy (DR) is the most frequent cause of blindness in working adults in the US. An estimated 9.6 million people in the U.S. are living with DR. Of these, 1.84 million have vision-threatening DR. This number is expected to double by 2050 (*1*). This condition is associated with neuronal and glial injury as well as vascular dysfunction (*2-6*). Laser photocoagulation is usually effective for advanced retinopathy but can impair vision and in some patients, retinopathy continues to progress. Intraocular injections of anti-VEGF antibodies have shown efficacy in reducing diabetic macular edema (*7*). However, the effectiveness of this treatment is limited in some cases and resistance to intravitreal anti-VEGF and recurrence of pathology have been reported (*8*). Also, anti-VEGF treatment does not promote tissue repair and may have adverse effects, including neuronal damage, retinal detachment, and intraretinal infection (*9*). Therefore, novel therapeutic strategies are urgently needed to limit injury and promote repair during DR.

Diabetes mellitus is a chronic metabolic disease characterized by dysfunctional insulin activity and high plasma glucose levels which lead to changes in glycogen and fatty acid metabolism followed by lipid accumulation and increased oxidative stress (*10, 11*). While results of studies

examining the link between DR and lipid abnormalities are inconsistent, one study found that high levels of circulating LDL cholesterol are associated with significant risk for diabetic macular edema and retinal hard exudates (*12*). Dyslipidemia has also been linked to faster progression and worsening of DR (*13*), (*14*). Also, studies of post-mortem retinas from DR patients have shown increases in oxidized LDL associated with macrophage infiltration and severity of DR (*15*), (*16*). In peripheral vascular disease, accumulation of CE stored as cytoplasmic lipid droplets is a major characteristic of macrophage foam cells that are central to the development of atherosclerotic plaques (*17*). Based on these findings, we hypothesized a pathophysiological role for CE formation in DR.

Our previous research has identified AcylCoA:cholesterol acyltransferase 1 (ACAT1/SOAT1) as a critical mediator of pathological retinal neovascularization (RNV) in a mouse model of oxygen-induced retinopathy (OIR) (*18*). ACAT1/SOAT1 is an endoplasmic reticulum membrane-bound enzyme that uses cholesterol and long chain fatty acid as substrates to produce CE (*19*). ACAT1/SOAT1 is expressed in many cell types, including photoreceptors, macrophages, monocytes, and microglial cells (*5, 20*). Our studies in the OIR mouse model have shown increases in lipid accumulation and CE formation in areas of pathological RNV. These increases were associated with significant elevation of ACAT1/SOAT1, macrophage colony stimulating factor (MCSF), LDL receptor (LDLR), and VEGF. Treatment with a specific inhibitor of ACAT1/SOAT1, K604, blocked increases in all these proteins except VEGF. Moreover, K604 treatment also inhibited RNV and improved vascular repair (*18*). In the present study we have tested the role of ACAT1/SOAT1 activity in neurovascular injury during DR. We hypothesized that diabetes causes high levels of retinal CE formation which activates inflammatory signaling pathways and therefore promotes neurovascular damage.

RESULTS

ACAT1/SOAT1 is upregulated and functionally active in human diabetic retinopathy

Analysis of human DR tissues revealed a robust upregulation of ACAT1/SOAT1 expression and activity. Immunolabeling of retinal sections from DR donors showed strong ACAT1/SOAT1 immunoreactivity in the photoreceptor outer segments and retinal pigment epithelium (RPE), in contrast to weak signal in non-diabetic controls, indicating diabetes-associated enzyme upregulation (**Fig. 1A**). Consistently, vitreous samples from patients with proliferative DR exhibited elevated CE levels, confirming enhanced ACAT1/SOAT1 activity in the diabetic retina (**Fig. 1B**).

Diabetes promotes dysregulation of lipid metabolism in the diabetic retina

To investigate the functional role of ACAT1/SOAT1 in diabetic retinopathy, we treated diabetic $Ins2^{Akita}$ mice with the selective ACAT1/SOAT1 inhibitor K604. To validate our experimental design, we first confirmed the onset of hyperglycemia in $Ins2^{Akita}$ mice at 5 weeks of age and established treatment regimens with the ACAT1/SOAT1 inhibitor K604 (**Supplementary Fig. 1A**). Intraperitoneal injections of K604 for 2 weeks did not affect body weight or blood glucose levels in the diabetic mice, indicating that any observed effects are independent of systemic metabolic changes (**Supplementary Fig. 1B, C**).

To determine whether diabetes alter cholesterol homeostasis in the retina, we assessed lipid and CE levels in $Ins2^{Akita}$ diabetic mouse retinas. Oil Red O staining showed a slight increase in lipid levels in the retinal ganglion cell layer and photoreceptor outer segments of the diabetic retinas, and this was not evident after K604 treatment. Quantitation of relative fluorescence intensity (RFI) showed no significant difference in the overall RFI. (**Fig. 2A, B**). Filipin staining demonstrated

106 prominent increases in CE deposition in multiple retinal layers of diabetic mice as compared with
107 the non-diabetic controls and these increases were blocked by K604 treatment (**Fig. 2C, D**).
108 Biochemical analysis further confirmed elevated CE levels in both retina (**Fig. 2E**) and plasma
109 (**Fig. 2F**) of $Ins2^{Akita}$ diabetic mice. These increases were blocked by K604 treatment. However,
110 levels of cholesterol were significantly increased only in plasma, but not in retina.

111 **ACAT1/SOAT1 inhibition normalizes expression of ACAT1/SOAT1 and suppresses**
112 **inflammatory and angiogenic signaling**.

113 Western blot analyses of $Ins2^{Akita}$ diabetic retinas demonstrated significant upregulation of LDLR
114 and ACAT1/SOAT1 and that this was accompanied by increased expression of inflammatory and
115 angiogenic mediators including TREM1, MCSF, VEGF, and TNFα. Treatment with K604 restored
116 expression of all these proteins to near-control levels, suggesting that ACAT1/SOAT1 activity
117 drives both increases of CE levels and activation of pathogenic inflammatory signaling cascades
118 in the diabetic retina (**Fig. 3A-G**). Increased levels of ACAT1/SOAT1 in the retinal ganglion cells,
119 outer segments, and RPE cells were also detected in retinal frozen sections from diabetic mice.
120 These pathological increases of ACAT1/SOAT1 were blocked by the K604 inhibitor treatment,
121 without interfering with their physiological expression (**Fig. 3H, I**).

122 **ACAT1/SOAT1 inhibition limits oxidative stress and retinal inflammation**

123 Markers of oxidative stress and inflammation were elevated in diabetic retinas, changes that were
124 mitigated by ACAT1/SOAT1 inhibition. DHE (dihydroethidium) imaging revealed that diabetes-
125 induced superoxide production in diabetic retinas was blocked in K604-treated animals (**Fig. 4A,**
126 **B**). Specificity of DHE fluorescence for superoxide was confirmed by preincubation with

127 superoxide dismutase (SOD), which completely abolished the diabetes-induced DHE signal,
128 (**Supplementary Fig. 2A, B**).

129 Labeling for the lipid peroxidation marker 4-hydroxynonenal (4-HNE) showed areas that were
130 increased in the RGC, photoreceptors and RPE layers of diabetic mice were reduced by K604
131 treatment (**Fig. 4C, D**). GFAP labeling also indicated Müller glial cell activation in diabetic retinas
132 (**Fig. 4E, F**) and this was blocked by the K604 treatment. Iba1 immunolabeling of retinal microglia
133 revealed enlarged, ameboid microglia and macrophages in the $Ins2^{Akita}$ diabetic retinas, but not in
134 eyes of K604 treated animals (**Supplementary Fig. 3**). At the transcriptional level, diabetic retinas
135 exhibited upregulation of *Acat1/Soat1* along with proinflammatory mediators including *Mcsf1*,
136 *Il1b*, *Tnfa*, and *Nos2*, all of which were suppressed by K604 administration (**Fig. 4G-K**).

137 **ACAT1/SOAT1 inhibition preserves visual function in early diabetes**

138 We next tested whether inhibiting ACAT1/SOAT1 confers neuroprotection. Confocal imaging of
139 retinal flat mounts labeled with the neuronal cell marker RBPMS showed that K604 treatment
140 increased the survival of retinal ganglion cells compared with vehicle-treated diabetic mice (**Fig.**
141 **5A, B**). Functional assessment using electroretinography (ERG) revealed that both scotopic a- and
142 b-wave amplitudes were significantly improved following K604 treatment, indicating preserved
143 photoreceptor and bipolar cell function (**Fig. 5C, D**). Moreover, visual acuity, measured by
144 optomotor responses (OMR), was markedly enhanced in K604-treated diabetic mice (**Fig. 5E**).
145 These findings demonstrate that the inhibition of ACAT1/SOAT1 preserves neuronal integrity and
146 visual function in the diabetic retina.

147 **ACAT1/SOAT1 inhibition preserves retinal microvascular integrity in early diabetes**

148 Diabetic mice exhibited characteristic microvascular abnormalities, including increased
149 leukostasis, vascular permeability, and acellular capillary formation, all of which were prevented
150 by ACAT1/SOAT1 inhibition. Quantitative analysis of attached leukocytes within the retinal
151 vessels showed enhanced leukocyte adhesion in diabetic mice and this increase was normalized
152 by K604 treatment (**Fig. 6A, B**). Vascular leakage, assayed by FITC-BSA fluorescence, was
153 markedly elevated in diabetic retinas but was strongly suppressed following inhibitor treatment
154 (**Fig. 6C, D**). Furthermore, K604 significantly blocked the diabetes-induced increase in acellular
155 capillaries, a hallmark of diabetic microvascular degeneration (**Fig. 6E, F**). These findings
156 demonstrate that ACAT1/SOAT1 activity contributes to retinal vascular pathology in diabetes and
157 that its inhibition preserves microvascular integrity.

158 **ACAT1/SOAT1 inhibition limits vascular leakage and preserves visual function in later stage**
159 **diabetic retinopathy**

160 To determine whether ACAT1/SOAT1 inhibition is effective at later stages of disease, 8-month-
161 old $Ins2^{Akita}$ mice were treated with K604 for 2 months (**Supplementary Fig. 4A**). As expected,
162 diabetes caused a reduction in body weight, which was not altered by K604 treatment
163 (**Supplementary Fig. 4B**). Blood glucose levels significantly increased in diabetic mice compared
164 with WT controls and remained unchanged following K604 treatment (**Supplementary Fig. 4C**).
165 Oil Red O (**Fig. 7A, B**) and filipin staining (**Fig. 7C, D**) revealed pronounced lipid accumulation
166 and cholesterol ester deposition in the ganglion cell layer, horizontal cell layers and photoreceptor
167 outer segments of diabetic retinas. These findings were associated with high levels of 4HNE in the
168 same location as CE deposition, indicating increases in lipid peroxidation. These alterations were
169 significantly reduced by ACAT1/SOAT1 inhibitor treatment **(Fig.7E, F).**

170 Western blot analyses further demonstrated marked increases in LDLR, ACAT1/SOAT1, and
171 TREM1 expression in diabetic retinas compared with non-diabetic controls, all of which were
172 normalized following K604 administration (**Fig. 7G-J)**). These results show that inhibiting
173 ACAT1/SOAT1 reduces lipid/cholesterol accumulation and inflammatory/oxidative signaling
174 even at advanced stages of diabetic retinopathy.

175 **K604 preserves vascular integrity and vision in late-stage DR**

176 We determined whether long-term ACAT1/SOAT1 inhibition preserves retinal vascular integrity
177 and function in advanced diabetic retinopathy. Albumin staining of retinal sections revealed
178 extensive vascular leakage surrounding retinal vessels positive for isolectin B_4 in diabetic retinas.
179 This was markedly reduced by K604 treatment (**Fig. 8A, B**). Consistent with improved vascular
180 integrity, optomotor response testing demonstrated a significant preservation of visual acuity in
181 K604-treated diabetic mice compared with vehicle-treated controls (**Fig. 8C**). Functional
182 assessment by ERG further showed preservation of the scotopic a- and b-wave amplitudes in
183 inhibitor-treated mice, indicating preserved photoreceptor and bipolar cell function (**Fig. 8D, E**).
184 These findings demonstrate that ACAT1/SOAT1 inhibition not only reduces vascular leakage but
185 also preserves visual function in later stages of diabetic retinopathy.

186 **Discussion**

187 Our studies demonstrate that diabetes induces increases in CE formation due to activation of
188 ACAT1/SOAT1, which in turn induces key components of DR, including increases in oxidative
189 stress, inflammation, vascular pathology, and neuronal dysfunction. Using the $Ins2^{Akita}$ model of
190 type 1 diabetes, we show that systemic treatment with the specific ACAT1/SOAT1 inhibitor K604
191 prevents CE accumulation, normalizes inflammatory and angiogenic signaling, protects against

192 microvascular and neuronal injury, and preserves visual function. Importantly, these effects were
193 observed in both early- and late-stage intervention paradigms, highlighting the therapeutic
194 potential of targeting cholesterol esterification across the spectrum of DR duration and
195 progression.

196 Our findings provide mechanistic insight into how dysregulated cholesterol metabolism
197 contributes to diabetic retinal pathology. We observed strong upregulation of ACAT1/SOAT1 and
198 LDLR in diabetic retinas, consistent with increased cholesterol uptake and esterification. The
199 increase in CE formation was associated with increases in oxidative stress, glial activation, and
200 elevated pro-inflammatory mediators including TREM1, MCSF, IL-1β, TNF-α, and VEGF.
201 Previous studies in models of atherosclerosis have shown that dyslipidemia triggers increased
202 TREM1 expression on myeloid cells. TREM1 is a potent amplifier of inflammatory signals (*21,*
203 *22*). It has been shown to trigger monopoiesis, production of pro-atherogenic cytokines, and foam
204 cell formation in atherosclerotic lesions (*23*). Our findings show that increases in ACAT1/SOAT1
205 activity, CE formation, and expression of TREM1 are linked to oxidative stress, upregulation of
206 inflammatory mediators, and retinal neurovascular dysfunction in the $Ins2^{Akita}$ diabetic mice retina
207 demonstrates a novel role of this pathway in DR.

208 This CE-driven inflammatory state aligns with previous reports linking dyslipidemia to DR
209 severity and provides a mechanistic explanation for the limited efficacy of systemic lipid-lowering
210 therapies in clinical trials. Unlike systemic statins or fibrate targeting therapies, ACAT1/SOAT1
211 inhibition directly targets intracellular cholesterol esterification within the retina, thereby reducing
212 the pool of bioactive lipids that fuel oxidative stress and inflammation. Identification of the specific
213 mechanisms by which increased CE formation promotes oxidative stress and expression of
214 TREM1, and other inflammatory mediators require further investigation. Studies in models of

215 cardiovascular disease have shown that oxidized CE can induce the activation of several
216 inflammatory mediators (*24*). While this mechanism is clearly established in cardiovascular
217 disease, its role in DR is completely unknown.

218 We also establish a critical link between cholesterol esterification and vascular dysfunction. K604
219 treatment prevented diabetes-induced leukostasis, vascular leakage, and acellular capillary
220 formation, suggesting that CE accumulation contributes to endothelial injury and blood–retina
221 barrier breakdown. These results are consistent with prior work implicating lipid peroxidation and
222 inflammatory signaling in retinal vascular dysfunction. Moreover, by reducing VEGF expression,
223 ACAT1/SOAT1 inhibition addresses one of the key drivers of pathological neovascularization in
224 proliferative DR.

225 Beyond vascular effects, we demonstrate that ACAT1/SOAT1 inhibition provides robust
226 neuroprotection. K604 treatment preserved retinal ganglion cell survival, improved ERG
227 responses, and enhanced visual acuity. This is particularly significant, as visual dysfunction often
228 precedes clinically detectable vascular lesions in DR. By targeting upstream metabolic
229 dysregulation, ACAT1/SOAT1 inhibition may intervene earlier in the disease course than current
230 anti-VEGF therapies, which primarily address late stage neovascular complications.

231 The protective effects of K604 were observed without changes in either systemic glucose levels or
232 body weight, confirming that the benefits were independent of glycemic control. We were not
233 expecting K604 to normalize glucose levels since $Ins2^{Akit}$ mice undergo a spontaneous mutation
234 of the *Ins2* gene resulting in early onset diabetes due to lack of insulin production (*25*). However,
235 further studies are needed to assess the effect of K604 on plasma glucose levels in different models
236 of diabetes. This is relevant clinically, as intensive glycemic control is often insufficient to fully
237 prevent progression of DR. Our findings suggest that adjunctive therapy targeting cholesterol

238 esterification complementing current glucose-lowering and anti-VEGF treatments may be helpful
239 in limiting DR.

240 There are several potential limitations to consider. First, our study was performed exclusively in
241 Ins2^{Akita} mouse, a model of type 1 diabetes, and it will be important to confirm these findings in
242 models of type 2 diabetes and in human retinal tissue. Second, while K604 is a selective
243 ACAT1/SOAT1 inhibitor, off-target effects cannot be fully excluded and development of more
244 retina-specific ACAT1/SOAT1 inhibitors would be desirable for clinical translation. Finally, long-
245 term safety studies are needed to determine whether chronic ACAT1/SOAT1 inhibition alters other
246 cholesterol-dependent pathways in the retina or peripheral tissues.

247 In conclusion, our work identifies ACAT1/SOAT1 as a key regulator of lipid-driven pathology in
248 diabetic retinopathy and establishes cholesterol esterification as a novel therapeutic target. By
249 reducing oxidative stress, inflammation, vascular and neuronal dysfunction, ACAT1/SOAT1
250 inhibition offers a multifaceted approach to DR treatment. These findings provide a strong
251 rationale for further preclinical development of ACAT1/SOAT1 inhibitors and may open new
252 avenues for treating both early and advanced stages of diabetic retinopathy.

253 Significance Statement

254 Diabetic retinopathy (DR) remains the leading cause of blindness in working-age adults, and
255 current therapies, including anti-VEGF injections, primarily target late-stage vascular
256 complications without addressing the underlying metabolic drivers of disease. Our study identifies
257 cholesterol esterification via ACAT1/SOAT1 as a central metabolic mechanism linking diabetes
258 to oxidative stress, inflammation, vascular injury, and neuronal dysfunction in the retina.
259 Pharmacologic inhibition of ACAT1/SOAT1 not only reduced vascular leakage and inflammation

260 but also preserved visual function, even when treatment was initiated at advanced disease stages.
261 These findings highlight cholesterol esterification as a novel, targetable pathway in DR
262 pathogenesis and provide preclinical proof-of-concept for ACAT1/SOAT1 inhibitors as adjunctive
263 or alternative therapies to current treatment strategies.

264 **METHODS**

265 **Human donor retinas**

266 Retinal tissue sections from human donors with proliferative diabetic retinopathy (PDR) and age
267 matched non-diabetic controls were purchased from National Disease Research Interchange
268 (NDRI, Philadelphia, PA). Sections were deparaffinized and immunolabeled as described in the
269 immunolocalization section. Patient information is provided in **supplementary table 1**.

270 **Human vitreous samples**

271 Samples were collected from patients undergoing pars plana vitrectomy (PPV) due to proliferative
272 diabetic retinopathy (PDR) with retinal detachment and patients undergoing PPV for reasons other
273 than PDR (chronic retinal detachment, open globe injury, or macular hole). Vitrectomy samples
274 were concentrated using Amicon Ultra 30k centrifuge filter devices (cat # UFC903008) and CE
275 levels were measured as previously described (*26*). Patient information is provided in
276 **supplementary table 2**.

277 **Mouse model of type 1 diabetes and drug treatment**

278 Experiments were performed in accordance with the ARVO Statement for the Use of Animals in
279 Ophthalmic and Vision Research and were approved by the institutional animal care and use
280 committee animal welfare. Ins2Akita Type 1 diabetic mice and littermate control mice were bred

281 in our facility. Mice were sacrificed at different ages for experimental endpoints and littermates
282 from the same cage were compared. Diabetes was confirmed by blood glucose measurement and
283 genotyping as previously described (*27*),(*28*). Mice were treated with intraperitoneal injections of
284 a specific ACAT1/SOAT1 inhibitor (K604, MedChem Express, 10 mg/Kg in PBS) or vehicle
285 control (PBS) every 2 days. One group of mice was treated for 2 weeks beginning at 10 weeks of
286 age and sacrificed at 3 months. Another group of mice was treated for 2 months beginning at 8
287 months and sacrificed at 10 months. Previous studies have shown that intraperitoneal injection of
288 K604 is safe and that the drug can penetrate the blood-retinal barrier (*18*).

289 **Western blotting**

290 Lysates from retina samples and cell lines were prepared for protein quantification and western
291 blot analysis following our established protocol (*29*). The samples were homogenized in modified
292 RIPA buffer (20 mM Tris–HCl, 2.5 mM EDTA, 50 mM NaF, 10 mM Na4P2O7, 1% Triton X-100,
293 0.1% sodium dodecyl sulfate, 1% sodium deoxycholate, 1 mM phenylmethylsulfonylfluoride, pH
294 7.4). Samples containing equal amounts of protein were separated by 10% or 12% sodium dodecyl
295 sulfate polyacrylamide gel electrophoresis, transferred to polyvinylidene difluoride (PVDF) or
296 nitrocellulose membrane, and reacted overnight with anti-LDLR, anti-ACAT1/SOAT1, anti-
297 TREM1, anti-MCSF1, anti-TNF-a, and anti-VEGF antibodies in 5% milk or 2% BSA, followed
298 by incubation with corresponding horseradish peroxidase-linked secondary antibodies. Bands
299 were quantified by densitometry, and the data were analyzed using ImageJ software. Equal loading
300 was verified by stripping the membranes and reproving them with a mouse monoclonal antibody
301 against β actin. Antibodies were obtained from various sources. Their catalog information, together
302 with working dilutions, is provided in **supplementary table 3**.

303

304 **Quantitative real time RT PCR (qRT PCR) analysis**

305 Total RNA from mouse retina samples was extracted with an RNAqueous 4PCR total RNA
306 isolation kit (Invitrogen, Carlsbad, CA, US), and qRT PCR was performed as described previously
307 (*18, 30*). Briefly, a 0.25 μg sample of RNA was utilized as a template for reverse transcription
308 using M-MLV reverse transcriptase (Invitrogen). qRT PCR was performed on an ABI 7500 Real
309 Time PCR System (Applied Biosystems, Foster City, CA) with the respective gene-specific
310 primers listed in **supplementary table 4**. The relative mRNA expression was calculated using the
311 comparative threshold cycle (ΔΔCt) method against the internal control, hypoxanthine
312 phosphoribosyl-transferase (HPRT). Expression levels for all genes are reported as fold change to
313 room air controls.

314 **Immunolocalization**

315 Retinal frozen sections and flat mounts were processed for immunolabeling according to our
316 standard protocol (*18, 31*). The samples were blocked with normal goat serum or donkey serum
317 and incubated overnight with IB_4, anti-Iba1, anti-GFAP, anti-ACAT1/SOAT1, and anti-4HNE
318 antibodies. The samples were washed 3 times with PBS and incubated with secondary antibodies
319 (Invitrogen, Waltham, MA). Antibodies were obtained from various sources, and their catalog
320 information, together with working dilutions, is provided in supplementary table 2. Tissue sections
321 were also reacted with secondary antibody alone to rule out non-specific reactivity. Images were
322 captured using a Zeiss Axioplan2 fluorescence microscope or Zeiss 780 inverted Confocal
323 microscope (Carl Zeiss Meditec, Inc. Dublin, CA).

324 **Oil Red O staining for detection of neutral lipids**

325 Cholesterol and other neutral lipids were detected as described previously (*18, 32*) . Retina frozen
326 sections were reacted with 0.5% Oil Red O (Sigma-Aldrich, St. Louis, MO, dissolved in 1,2-
327 isopropanol, 15 min, room temperature), rinsed in 60% 2-propanol for 5 min and rinsed in distilled
328 water (twice, 5 min each time). Sections were mounted in aqueous mounting media to capture the
329 images using a Zeiss Axioplan 2 fluorescence microscope (Carl Zeiss Meditec, Inc., Dublin, CA)
330 equipped with a 420 nm excitation filter, 520 nm barrier filter, and a 20× lens.

331 **Filipin staining for detection cholesterol ester**

332 Retinal frozen sections were reacted with the fluorescent polyene antibiotic filipin (Sigma-Aldrich,
333 St. Louis, MO) to detect CE. This compound binds specifically to sterols and interacts with the 3-
334 β hydroxyl group of cholesterol. For CE detection, we followed the protocol described by Rudolf
335 and Curcio (*33*). Native unesterified cholesterol (UC) was extracted from cryosections by rinsing
336 in 60% ethanol for 10 min. Native CE was hydrolyzed with cholesterol esterase (1.65 units/mL)
337 in PBS for 3 h at 37 °C (C9281, Sigma St. Louis, MO). The newly released UC by the hydrolysis
338 of CE was stained with 50 ng/mL filipin in PBS for about 60 min in the dark at room temperature.

339 **Cholesterol ester measurement by ELISA**

340 Levels of CE formation were determined as described previously (*18*) using the luminescence-
341 based Cholesterol/Cholesterol Ester Glo™ Assay (J3190, Promega, Madison, WI) according to the
342 manufacturers' protocol. Briefly, human vitreous samples and mouse retinas were collected and
343 homogenized, and blood plasma was collected. All samples were diluted (1:10) in cholesterol lysis
344 solution and incubated at 37 °C for 30 min. Equal amounts of extracts were incubated in cholesterol
345 detection reagent with and without cholesterol esterase enzyme in 96 well white bottom plates at
346 room temperature for 1 h. Luminescence was recorded using a Polar Star Omega microplate reader

347 (BMG Labtech Inc, NC). Total and free cholesterol concentrations were measured by comparing
348 the luminescence of samples with and without cholesterol esterase, respectively. Concentrations
349 of CE were calculated as the difference between total and free cholesterol concentrations.

350 **ROS production**

351 The dihydroethedium (DHE) method was used to evaluate superoxide formation as described
352 previously (*34, 35*). Briefly, fresh frozen sections were preincubated with or without SOD-
353 polyethylene glycol (400 U/ml, Sigma-Aldrich, St. Louis, MO, USA) for 30 min, followed by
354 reaction with DHE (10 μM) for 15 min at 37 °C. Superoxide, the absence of SOD, oxidizes DHE
355 to ethidium bromide, which binds to DNA and fluoresces red (*36*). A fluorescence microscope
356 (AxioVision; Carl Zeiss) was used to obtain the DHE images immediately after incubation. DHE
357 was excited at 488 nm with an emission spectrum of 610 nm. Six images per slide were taken and
358 the relative fluorescence intensity was measured by ImageJ software.

359 **Isolation of the retinal vasculature and measurement of acellular capillaries**

360 The trypsin digestion method was used for isolating the retinal vasculature as previously described
361 with minor modification(*35*). Eyeballs were removed and fixed with 4% paraformaldehyde
362 overnight. Retinas were carefully dissected and incubated in distilled water at room temperature
363 with gentle shaking for at least 24 h. Then the retinas were digested with 3% trypsin (Difco Trypsin
364 250, Becton Dickinson and Company, Sparks, MD, USA) in 0.1 M Tris buffer (pH 7.8) for 1.5 h
365 at 37°C on an orbital shaker (50 r.p.m.). Retinas were washed carefully in several changes of fresh
366 distilled water until no non-vascular tissue was observed under the microscope. The isolated retinal
367 vasculature was air-dried on silane-coated slides and stained with periodic acid–Schiff and
368 hematoxylin. Acellular capillaries were counted in 10 random areas of the mid-retina. The field

369 area was calculated using ImageJ software. The numbers of acellular capillaries were divided by
370 the field area to get number of acellular capillaries per/mm^2 of retina.

371 **Retinal vascular permeability**

372 Retinal vascular permeability was tested by evaluating albumin extravasation into the retinal
373 parenchyma using albumin staining on retinal cross sections as described previously (*29*). Mice
374 received intraperitoneal injections of 10 mg/Kg bovine serum albumin (BSA)–Alexa-Fluor 488
375 conjugate (Invitrogen-Molecular Probes, Eugene, OR). After 2 hours, a thoracotomy was
376 performed on deeply anesthetized mice. The right atrium was cut, and a heparinized catheter was
377 inserted into the left ventricle. Mice were perfused transcardially with PBS 1X at 37° C for 2
378 minutes to wash out the BSA-Alexa-Fluor 488 from the retinal vessels. Eyeballs were enucleated
379 and fixed overnight in 4% paraformaldehyde in PBS at 4 °C. The retinas were dissected into whole
380 mounts and images were acquired using a fluorescence microscope (Keyence, BZ-X700). The
381 images of the whole retinal flat mounts were constructed by capturing a series of 6 pictures from
382 all samples using a 4× lens. Fluorescence intensity was quantified using Image J.

383 Other eyeballs were embedded in OCT compound for preparation of frozen sections which were
384 reacted with a rabbit anti-mouse albumin antibody (1:400, Bethyl Laboratory) followed by reaction
385 with Oregon green labeled goat anti-rabbit antibody (1:500; Invitrogen). Fluorescence images
386 were acquired using a fluorescence microscope and relative intensity of extravascular albumin was
387 measured by ImageJ.

388 **Leukocyte Adhesion**

389 Adhesion of leukocytes to the wall of the retinal vessels was evaluated as described previously(*31*).
390 After the induction of deep anesthesia, the chest cavity was carefully opened, and a 20-gauge

391 perfusion cannula was introduced into the aorta. Drainage was achieved by opening the right
392 atrium. The animals were then perfused with 10 mL of phosphate-buffered saline (PBS) to wash
393 out nonadherent blood cells. Next, the animals were perfused with 10 mL fluorescent
394 isothiocyanate (FITC)–labeled concanavalin A (Con A) lectin (40 μg/mL in PBS, pH 7.4; Vector
395 Laboratories, Burlingame, CA) to label the adherent leukocytes and vascular endothelial cells.
396 Residual unbound Con A was removed by right ventricle perfusion with PBS at a rate of 1.8 ml
397 per minute to temperature of 37^0C. Eyeballs were enucleated and fixed overnight in 4%
398 paraformaldehyde in PBS at 4 °C. The retinas were dissected into flat mounts, analyzed by
399 fluorescence Keyence microscopy, and the total number of adherent leukocytes per retina was
400 calculated

401 **Wholemount retina and GCL neuronal cell counting**

402 Neuronal degeneration was assessed as previously described (*37, 38*) Eyeballs were enucleated
403 and fixed overnight in 4% paraformaldehyde in PBS at 4 °C. Retinas were dissected into flat
404 mounts and incubated with the neuronal marker anti-RBPMS antibody overnight at 4 °C and then
405 incubated with Alexa fluor 488 conjugated secondary antibodies. Four images were taken in the
406 midperiphery region of each retina flat mount using a Keyence fluorescence microscope and
407 numbers of RBPMS-positive cells were calculated using ImageJ software. Data are represented as
408 numbers of RBPMS-positive cells in the GCL per mm^2.

409 **OptoMotry**

410 OptoMotry (Cerebral Mechanics Inc.) was employed for screening visual function using the
411 optokinetic tracking (OKT) response (*39, 40*) (*41*). Individual unrestrained mice were placed on
412 an elevated platform surrounded by four computer monitors. The monitors project a virtual

413 stimulus in the form of a sine wave that rotates around the animal. Animals track the grating with
414 reflexive head and neck movements in the direction of grid rotation. By reversing the direction of
415 the grid rotation, the system measures visual function in each eye separately because motion in the
416 temporal to nasal direction of either eye elicits a tracking response. A camera monitors the behavior
417 of the animal from above, allowing the observer to detect the mouse tracking responses in real
418 time and give a score of yes or no. The whole study was conducted by an observer who was blinded
419 to the treatment groups. To examine visual acuity, spatial frequency thresholds (cycles per degree)
420 were measured by systematically increasing the spatial frequency of the grating (decreasing the
421 bar width) at full contrast until mice no longer tracked. Rotation speed was fixed at 12 degrees per
422 second, and the data was managed and generated by the software. Data are presented as responses
423 from both eyes.

424 **Electroretinography (ERG)**

425 ERG was performed to investigate neuronal functions using the Celeris-Diagnosys system
426 (Diagnosys, Lowell, MA, USA) as described previously (*41*). After overnight dark adaptation,
427 mice were anesthetized and pupils were dilated with topical 0.5% tropicamide (Akorn, Lake
428 Forest, IL, USA) and 2.5% phenylephrine HCL (Paragon BioTeck, Portland, OR, USA). Mouse
429 corneas were then moisturized with a thin layer of GenTeal Lubricant Eye Gel (Alcon, Ft. Worth,
430 TX). The light guide electrodes were placed on the gel and recording began after the scotopic and
431 photopic testing was set up. For each animal, the light guide electrode was used to present light
432 flashes over a range of intensities and record ERG responses. The a-wave amplitude was measured
433 as the difference between the pre-stimulus baseline and the trough of the a-wave. The b-wave
434 amplitude was measured from the trough of the a-wave to the peak of the b-wave. The results are
435 presented as average values of amplitude with the two eyes of each mouse.

436 **Statistical analysis**

437 All data were analyzed by investigators blinded to the group allocation. Differences among the
438 groups were compared by an independent two sample t test for two groups or one-way ANOVA
439 followed by a post hoc test for multiple comparisons. Values are represented as means ± standard
440 error of the means (SEM). P values of less than 0.05 were considered significant.

441 **List of Supplementary Materials**

442 Supplementary figures 1 to 4 for multiple supplementary figures.

443 Supplementary table 1 to 4 for multiple supplementary tables.

444 **Acknowledgements**: Dr. Ta-Yuan Chang, Ph.D. and Dr. Catherine Chang from Dartmouth Geisel
445 School of Medicine, Hanover, New Hampshire, Dr. Eric J. Belin de Chantemèle from Vascular
446 Biology Center Augusta University, Augusta Georgia, Dhruvi Paladiya, Medical College of
447 Georgia, Augusta GA.

448 **Funding**: This study was supported by grants from the National Institute of Health
449 [R01EY035683, R01EY011766, R01EY030500, P30EY031631] and the Culver Vision Discovery
450 Institute at Augusta University.

451 **Author contribution:**

452 Conceptualization: MAR
453 Methodology: MAR, SAHZ, RBC
454 Investigation: MAR, SAHZ, RBC, TL, XZ
455 Visualization: MAR
456 Funding acquisition: MAR, RBC

457 Project administration: RBC

458 Supervision: MAR

459 Writing – original draft: SAHZ, MAR, RBC, MY

460 Writing – review & editing: MAR, RBC, WRC, SB, MY

461

462 **Competing interests:** The authors declare that they have no competing interests.

463 **Data and materials availability:** The data generated and/or analyzed during the current study are
464 available from the corresponding authors on reasonable request.

465 **Declarations**

466 Ethics approval and consent to participate

467 All experiments were conducted in accordance with the ARVO Statement for the Use of Animals
468 in Ophthalmic and Vision Research and were approved by the Augusta University Institutional
469 Animal Care and Use Committee (animal protocol # 2008-0243).

470 Human tissues were from donors who had given consent for the use of the tissues for research
471 purposes.

472 **Figures legend**

473 **Fig.1. ACAT1/SOAT1 expression and activity are upregulated in retina and vitrectomy**
474 **samples from patients with diabetic retinopathy (DR).**

475 **A.** Immunolabeling of retina sections from human donors with DR showed increased
476 ACAT1/SOAT1 immunoreactivity in the photoreceptor outer segments (OS) and retinal pigment
477 epithelial (RPE) cells, as compared with non-diabetic control donors. Donor sample information

478 is provided in supplementary table 1. Scale bar = 50 µm. n=3. **B.** Vitrectomy tissues collected from
479 patients with PDR showed an increased level of CE, as measured by ELISA. Donor sample
480 information is provided in supplementary table 2. Data are presented as mean ± SEM; n=4-5;
481 **p<0.01.

482 **Fig.2. Inhibition of ACAT1/SOAT1 prevents diabetes-induced CE formation in Ins2^{Akita}**
483 **mice.** Ten-week old male diabetic Ins2^{Akita} mice were treated with PBS as vehicle or
484 ACAT1/SOAT1 inhibitor, K604 (10mg/Kg, i.p.), every 2 days for 2 weeks. After 2 weeks of
485 treatment, eyeballs and retinas were collected. **A-B.** Oil red O staining of frozen sections shows
486 mild reactivity in the ganglion cell layer (GCL) and photoreceptor outer segments (OS) of the
487 Ins2^{Akita} diabetic retina. Treatment with the ACAT1/SOAT1 inhibitor, K604, reduced this activity.
488 Mean ± SEM; n=4-5; *p<0.05; ns: not significant. **C-D.** Detection of CE by filipin labeling of
489 frozen retina sections shows prominent increases in CE formation in the ganglion cell (GCL), outer
490 plexiform (OPL) and photoreceptor outer segment (OS) layers of the Ins2^{Akita} diabetic retina.
491 Treatment with K604 prevented the CE increase. Scale bar = 40 µm; mean ± SEM; n=4;
492 ****p<0.0001. **E-F.** Total cholesterol and CE levels were measured in retinas and plasma from
493 non-diabetic control mice, Ins2^{Akita} diabetic mice, and K604-treated Ins2^{Akita} diabetic mice. This
494 analysis showed upregulation of total cholesterol in plasma of the Ins2^{Akita} mice but not in retina.
495 However, CE was increased in both retina and plasma of the Ins2^{Akita} mice. K604 treatment
496 reduced retinal CE formation as well as preventing the increases in both cholesterol and CE in
497 plasma. Data are presented as mean ± SEM; n=4-6; **p<0.01; ***p<0.001; ****p<0.0001; ns:
498 not significant.

499 **Fig.3. Inhibition of ACAT1/SOAT1 prevents diabetes-induced increases in expression of**
500 **inflammatory mediators and ACAT1/SOAT1 in Ins2^{Akita} mice. A.** Western blot analysis of

501 retinas from 12-week diabetic Ins2^{Akita} mice showed marked increases in **B.** LDLR, **C.**
502 ACAT1/SOAT1, **D.** TREM1, **E.** MCSF, **F.** VEGF, and **G.** TNF-α as compared with the WT non-
503 diabetic controls. These increases were normalized by the treatment with K604 (10mg/Kg, ip)
504 every two days from 10 to 12 weeks. Mean ± SEM, n=3-6; *p<0.05; **p<0.01; ***p<0.001;
505 ****p<0.0001. **H-I**. Increased immunoreactivity for ACAT1/SOAT1 was detected in retinal frozen
506 sections from Ins2^{Akita} diabetic mice, especially in the RGC, OPL, and OS layers. The ACAT1
507 immunoreactivity was significantly reduced in retinas of Ins2^{Akita} diabetic mice treated with K604.
508 Data are presented as mean ± SEM; n=3-6; Scale bar = 25 μm.

509 **Fig.4. Inhibition of ACAT1/SOAT1 ameliorates the diabetes-induced increases in oxidative**
510 **stress, gliosis, and expression of inflammatory mediators in Ins2^{Akita} mice. A-B.** DHE imaging
511 showed upregulation of superoxide formation in frozen sections from Ins2^{Akita} diabetic mice. This
512 effect was blocked by the K604 treatment. n=4. **C-D.** Immunofluorescent labeling of frozen retina
513 sections with 4-hydroxynonenal (4-HNE) and fluorescence intensity quantification showed
514 increased 4-HNE levels in the ganglion cell layer (GCL), outer plexiform layer (OPL) and
515 photoreceptor outer segments (OS) of the Ins2^{Akita} mice. K604 treatment blocked this effect. n=4.
516 **E-F.** Immunolabeling of retina cross-sections showed increased GFAP immunoreactivity in Müller
517 cells of the Ins2^{Akita} mice, which was blocked in the K604 treated mice. n=4. Scale bar=30 μm. **G-**
518 **K.** Quantitative RT-PCR showed upregulation of *Acat1/Soat1*, along with proinflammatory
519 mediators – *Mcsf1, Il1b, Tnfa*, and *Nos2* in Ins2^{Akita} diabetic mouse retinas, compared to non-
520 diabetic controls. K604 treatment significantly inhibited these increases. n=4-6. All the data are
521 presented as mean ± SEM. *p<0.05; **p<0.01; ***p<0.001; ****p<0.0001.

522 **Fig.5. Inhibition of ACAT1/SOAT1 limits retinal ganglion cell loss and improves visual**
523 **function in Ins2^{Akita} diabetic mice.** Ten-week-old male diabetic Ins2^{Akita} mice were treated with

524 ACAT1/SOAT1 inhibitor, K604 (10 mg/Kg, ip), every 2 days for 2 weeks. After 2 weeks, retinas
525 were collected for analysis **A-B.** Confocal imaging of retinal flat mounts labeled with the neuronal
526 marker, RBPMS and quantification showed a significant decrease in RPBMS positive retinal
527 ganglion cells in vehicle-treated $Ins2^{Akita}$ diabetic retinas compared to the non-diabetic control
528 retinas. This retinal ganglion cell loss was markedly reduced by the K604 treatment. n=5-6; scale
529 bar=40 μm. Data are presented as mean ± SEM. **C-D**. Retinal function was measured by
530 electroretinography (ERG). Both scotopic a-wave and scotopic b-wave were improved in K604-
531 treated $Ins2^{Akita}$ diabetic mice as compared with the vehicle treated diabetic mice. n=12–26. Data
532 are presented as mean ± SEM. **p<0.01 non-diabetic versus vehicle-treated diabetic mice; p<0.01
533 vehicle-treated diabetic versus K604-treated diabetic mice. **E**. Measurement of visual acuity by
534 optoMotry responses (OMR) showed a marked improvement in the K604-treated diabetic mice as
535 compared with the vehicle-treated diabetic mice. n=10-13. Data are presented as mean ± SEM.
536 *p<0.05; ***p<0.0001.

537 **Fig.6. Inhibition of ACAT1/SOAT1 prevents diabetes-induced microvascular abnormalities**
538 **(leukostasis, vascular permeability and acellular capillaries) in $Ins2^{Akita}$ diabetic mice.** Ten
539 week old male diabetic $Ins2^{Akita}$ mice were treated with ACAT1/SOAT1 inhibitor, K604 (10
540 mg/Kg, ip), every 2 days for 2 weeks. After the 2 weeks treatment, retinas were collected for
541 analysis. **A-B.** Quantitative analysis shows diabetes-induced increases in leukocyte adhesion in
542 $Ins2^{Akita}$ retinal vessels, which were significantly prevented by K604 treatment as compared with
543 vehicles. Data are presented as mean ± SEM. n=5-6; *p<0.05; **p<0.01; Scale bar=50 μm. **C-D**.
544 Vascular leakage was visualized and quantified by measuring the fluorescence intensity of FITC-
545 conjugated BSA. K604 treatment significantly prevented vascular leakage in $Ins2^{Akita}$ mice as
546 compared with vehicle controls. Data are presented as mean ± SEM. n=5-6; scale bar=300 μm;

547 ****p<0.0001. **E**. K604 treatment significantly prevented diabetes-induced increases in acellular
548 capillary formation as compared with the vehicle controls. Data are presented as mean ± SEM.
549 n=6, scale bar=40 μm; ****p<0.001.

550 **Fig.7. Inhibition of ACAT1/SOAT1 limits the progression of later stage DR-induced**
551 **lipid/cholesterol accumulation and inflammation.** Eight-months-old male $Ins2^{Akita}$ diabetic
552 mice were treated with ACAT1/SOAT1 inhibitor, K604 (10 mg/Kg, ip), every 2 days for 2 months.
553 After the 2 months treatment, retinas were collected for analysis. Oil red O staining (**A, B**), filipin
554 staining (**C, D**) and 4HNE staining (**E, F**) of frozen sections shows a strong reaction in areas of
555 the ganglion cell layer (GCL) and photoreceptor outer segments (OS) of the DR retina, indicating
556 lipid accumulation, CE formation, and oxidative stress, respectively. Treatment with the
557 ACAT1/SOAT1 inhibitor, K604, significantly blocked these effects. Scale bar=25 μm. Data are
558 presented as mean ± SEM; n=3-4; **p<0.01; ***p<0.001; ****p<0.0001. **G-J.** Western blot
559 analysis of retinal samples from the $Ins2^{Akita}$ diabetic mice showed marked increases in LDLR,
560 ACAT1/SOAT1, and TREM1, as compared with the WT non-diabetic controls. These increases
561 were normalized by treatment with K604. Mean ± SEM; n=3; *p<0.05; ***p<0.001;
562 ****p<0.0001.

563 **Figure 8. ACAT1/SOAT1 inhibitor treatment limits vascular leakage and preserves visual**
564 **function in later stage DR.** Eight-months old male $Ins2^{Akita}$ diabetic mice were treated with
565 ACAT1/SOAT1 inhibitor, K604 (10 mg/Kg, ip), every 2 days for 2 months. After 2 months, retinas
566 were collected for analysis. **A-B**. Albumin staining of retina sections showed a strong reaction in
567 areas of Isolectin B4-positive blood vessels in the diabetic retina, indicating vascular leakage.
568 Treatment with ACAT1/SOAT1 inhibitor, K604, significantly blocked this effect. Scale bar=25
569 μm; data are presented as mean ± SEM; n=3-4; *p<0.05; ****p<0.0001. **C**. Measurement of visual

570 acuity by optoMotry responses (OMR) showed a significant impairment in the vehicle-treated
571 diabetic Ins2^{Akita} mice that was significantly blunted in the K604-treated diabetic mice. n=6-10.
572 Data are presented as mean ± SEM; **p<0.01; ****p<0.0001. **D-E**. Electroretinography (ERG)
573 showed improvement in both scotopic a-wave and scotopic b-wave in K604-treated diabetic mice
574 as compared with the vehicle treated diabetic mice. n=6-10. Data are presented as mean ± SEM.
575 **p<0.01 non-diabetic versus vehicle-treated diabetic mice; p<0.01 vehicle-treated diabetic versus
576 K604-treated diabetic mice.

577

578 **REFERENCES**

579 1. NEI, Projections for Diabetic Retinopathy (2010-2030-2050).
580 https://nei.nih.gov/eyedata/diabetic#5, (2010).
581 2. N. N. Osborne, R. J. Casson, J. P. Wood, G. Chidlow, M. Graham, J. Melena, Retinal
582 ischemia: mechanisms of damage and potential therapeutic strategies. *Prog Retin*
583 *Eye Res* **23**, 91-147 (2004).
584 3. A. B. Fulton, R. M. Hansen, A. Moskowitz, J. D. Akula, The neurovascular retina in
585 retinopathy of prematurity. *Prog Retin Eye Res* **28**, 452-482 (2009).
586 4. A. J. Barber, T. W. Gardner, S. F. Abcouwer, The significance of vascular and neural
587 apoptosis to the pathology of diabetic retinopathy. *Invest Ophthalmol Vis Sci* **52**,
588 1156-1163 (2011).
589 5. C. Altmann, M. H. H. Schmidt, The Role of Microglia in Diabetic Retinopathy:
590 Inflammation, Microvasculature Defects and Neurodegeneration. *Int J Mol Sci* **19**,
591 (2018).

592 6. E. Kovoor, S. K. Chauhan, A. Hajrasouliha, Role of inflammatory cells in
593 pathophysiology and management of diabetic retinopathy. *Surv Ophthalmol* **67**,
594 1563-1573 (2022).
595 7. B. P. Nicholson, A. P. Schachat, A review of clinical trials of anti-VEGF agents for
596 diabetic retinopathy. *Graefes Arch Clin Exp Ophthalmol* **248**, 915-930 (2010).
597 8. R. T. Atawia, K. L. Bunch, A. Y. Fouda, T. Lemtalsi, W. Eldahshan, Z. Xu, A. Saul, K.
598 Elmasry, M. Al-Shabrawey, R. B. Caldwell, R. W. Caldwell, Role of Arginase 2 in
599 Murine Retinopathy Associated with Western Diet-Induced Obesity. *J Clin Med* **9**,
600 (2020).
601 9. K. G. Falavarjani, Q. D. Nguyen, Adverse events and complications associated with
602 intravitreal injection of anti-VEGF agents: a review of literature. *Eye (Lond)* **27**, 787-
603 794 (2013).
604 10. T. W. Gardner, S. F. Abcouwer, A. J. Barber, G. R. Jackson, An integrated approach to
605 diabetic retinopathy research. *Arch Ophthalmol* **129**, 230-235 (2011).
606 11. A. S. ValdezGuerrero, J. C. Quintana-Perez, M. G. Arellano-Mendoza, F. J. Castaneda-
607 Ibarra, F. Tamay-Cach, D. Aleman-Gonzalez-Duhart, Diabetic Retinopathy:
608 Important Biochemical Alterations and the Main Treatment Strategies. *Can J*
609 *Diabetes* **45**, 504-511 (2021).
610 12. Y. C. Chang, W. C. Wu, Dyslipidemia and diabetic retinopathy. *Rev Diabet Stud* **10**,
611 121-132 (2013).

612 13. Z. Fu, C. T. Chen, G. Cagnone, E. Heckel, Y. Sun, B. Cakir, Y. Tomita, S. Huang, Q. Li,
613 W. Britton, S. S. Cho, T. S. Kern, A. Hellström, J. S. Joyal, L. E. Smith, Dyslipidemia in
614 retinal metabolic disorders. *EMBO Mol Med* **11**, e10473 (2019).
615 14. J. V. Busik, Lipid metabolism dysregulation in diabetic retinopathy. *J Lipid Res* **62**,
616 100017 (2021).
617 15. M. Wu, Y. Chen, K. Wilson, A. Chirindel, M. A. Ihnat, Y. Yu, M. E. Boulton, L. I.
618 Szweda, J. X. Ma, T. J. Lyons, Intraretinal leakage and oxidation of LDL in diabetic
619 retinopathy. *Invest Ophthalmol Vis Sci* **49**, 2679-2685 (2008).
620 16. J. Y. Yu, T. J. Lyons, Modified Lipoproteins in Diabetic Retinopathy: A Local Action in
621 the Retina. *J Clin Exp Ophthalmol* **4**, (2013).
622 17. M. Ouimet, T. J. Barrett, E. A. Fisher, HDL and Reverse Cholesterol Transport. *Circ*
623 *Res* **124**, 1505-1518 (2019).
624 18. S. A. H. Zaidi, T. Lemtalsi, Z. Xu, I. Santana, P. Sandow, L. Labazi, R. W. Caldwell, R.
625 B. Caldwell, M. A. Rojas, Role of acyl-coenzyme A: cholesterol transferase 1 (ACAT1)
626 in retinal neovascularization. *J Neuroinflammation* **20**, 14 (2023).
627 19. Q. Hai, J. D. Smith, Acyl-Coenzyme A: Cholesterol Acyltransferase (ACAT) in
628 Cholesterol Metabolism: From Its Discovery to Clinical Trials and the Genomics Era.
629 *Metabolites* **11**, (2021).
630 20. A. Miyazaki, N. Sakashita, O. Lee, K. Takahashi, S. Horiuchi, H. Hakamata, P. M.
631 Morganelli, C. C. Chang, T. Y. Chang, Expression of ACAT-1 protein in human
632 atherosclerotic lesions and cultured human monocytes-macrophages. *Arterioscler*
633 *Thromb Vasc Biol* **18**, 1568-1574 (1998).

634 21. P. Pan, X. Liu, L. Wu, X. Li, K. Wang, X. Wang, X. Zhou, Y. Long, D. Liu, L. Xie, L. Su,
635 TREM-1 promoted apoptosis and inhibited autophagy in LPS-treated HK-2 cells
636 through the NF-kappaB pathway. *Int J Med Sci* **18**, 8-17 (2021).
637 22. R. Aydogan Baykara, T. R. Kiran, O. Otlu, M. Erdem, N. Pihtili Tas, Could TREM-1 be a
638 novel marker in the diagnosis of fibromyalgia?: A cross-sectional study. *Medicine*
639 *(Baltimore)* **103**, e38806 (2024).
640 23. D. Zysset, B. Weber, S. Rihs, J. Brasseit, S. Freigang, C. Riether, Y. Banz, A. Cerwenka,
641 C. Simillion, P. Marques-Vidal, A. F. Ochsenbein, L. Saurer, C. Mueller, TREM-1 links
642 dyslipidemia to inflammation and lipid deposition in atherosclerosis. *Nat Commun*
643 **7**, 13151 (2016).
644 24. A. Gonen, Y. I. Miller, From Inert Storage to Biological Activity-In Search of Identity for
645 Oxidized Cholesteryl Esters. *Front Endocrinol (Lausanne)* **11**, 602252 (2020).
646 25. R. Undi, H. Y. Lim, W. Wang, Rapid and reliable identification of insulin 2 gene
647 mutation in Akita diabetic mice by a tetra-primer-ARMS-PCR method. *Heliyon* **5**,
648 e01112 (2019).
649 26. A. Y. Fouda, Z. Xu, J. Suwanpradid, M. Rojas, E. Shosha, T. Lemtalsi, C. Patel, J. Xing,
650 S. A. Zaidi, W. Zhi, B. K. Stansfield, P. N.-M. Cheng, S. P. Narayanan, R. W. Caldwell,
651 R. B. Caldwell, Targeting proliferative retinopathy: Arginase 1 limits vitreoretinal
652 neovascularization and promotes angiogenic repair. *Cell Death & Disease* **13**, 745
653 (2022).
654 27. H. A. Toque, K. P. Nunes, L. Yao, Z. Xu, D. Kondrikov, Y. Su, R. C. Webb, R. B.
655 Caldwell, R. W. Caldwell, Akita spontaneously type 1 diabetic mice exhibit elevated

656 vascular arginase and impaired vascular endothelial and nitrergic function. *PLoS*
657 *One* **8**, e72277 (2013).
658 28. E. Shosha, L. Qin, T. Lemtalsi, S. A. H. Zaidi, M. Rojas, Z. Xu, R. W. Caldwell, R. B.
659 Caldwell, A. Y. Fouda, Investigation of Retinal Metabolic Function in Type 1 Diabetic
660 Akita Mice. *Front Cardiovasc Med* **9**, 900640 (2022).
661 29. M. Rojas, W. Zhang, Z. Xu, T. Lemtalsi, P. Chandler, H. A. Toque, R. W. Caldwell, R. B.
662 Caldwell, Requirement of NOX2 expression in both retina and bone marrow for
663 diabetes-induced retinal vascular injury. *PLoS One* **8**, e84357 (2013).
664 30. A. Y. Fouda, W. Eldahshan, Z. Xu, T. Lemtalsi, E. Shosha, S. A. Zaidi, A. A.
665 Abdelrahman, P. N. Cheng, S. P. Narayanan, R. W. Caldwell, R. B. Caldwell,
666 Preclinical investigation of Pegylated arginase 1 as a treatment for retina and brain
667 injury. *Exp Neurol* **348**, 113923 (2022).
668 31. M. Rojas, W. Zhang, D. L. Lee, M. J. Romero, D. T. Nguyen, M. Al-Shabrawey, N. T.
669 Tsai, G. I. Liou, M. W. Brands, R. W. Caldwell, R. B. Caldwell, Role of IL-6 in
670 angiotensin II-induced retinal vascular inflammation. *Invest Ophthalmol Vis Sci* **51**,
671 1709-1718 (2010).
672 32. H. Huang, Y. Liu, L. Wang, W. Li, Age-related macular degeneration phenotypes are
673 associated with increased tumor necrosis-alpha and subretinal immune cells in
674 aged Cxcr5 knockout mice. *PLoS One* **12**, e0173716 (2017).
675 33. M. Rudolf, C. A. Curcio, Esterified cholesterol is highly localized to Bruch's
676 membrane, as revealed by lipid histochemistry in wholemounts of human choroid. *J*
677 *Histochem Cytochem* **57**, 731-739 (2009).

678 34. J. Suwanpradid, M. Rojas, M. A. Behzadian, R. W. Caldwell, R. B. Caldwell, Arginase
679 2 deficiency prevents oxidative stress and limits hyperoxia-induced retinal vascular
680 degeneration. *PLoS One* **9**, e110604 (2014).
681 35. E. Shosha, Z. Xu, H. Yokota, A. Saul, M. Rojas, R. W. Caldwell, R. B. Caldwell, S. P.
682 Narayanan, Arginase 2 promotes neurovascular degeneration during
683 ischemia/reperfusion injury. *Cell Death Dis* **7**, e2483 (2016).
684 36. F. J. Miller, Jr., D. D. Gutterman, C. D. Rios, D. D. Heistad, B. L. Davidson, Superoxide
685 production in vascular smooth muscle contributes to oxidative stress and impaired
686 relaxation in atherosclerosis. *Circ Res* **82**, 1298-1305 (1998).
687 37. Z. Xu, A. Y. Fouda, T. Lemtalsi, E. Shosha, M. Rojas, F. Liu, C. Patel, R. W. Caldwell, S.
688 P. Narayanan, R. B. Caldwell, Retinal Neuroprotection From Optic Nerve Trauma by
689 Deletion of Arginase 2. *Front Neurosci* **12**, 970 (2018).
690 38. S. A. H. Zaidi, Z. Xu, T. Lemtalsi, P. Sandow, S. Athota, F. Liu, S. Haigh, Y. Huo, S. P.
691 Narayanan, D. J. R. Fulton, M. A. Rojas, A. Y. Fouda, R. W. Caldwell, R. B. Caldwell,
692 Calbindin 2-specific deletion of arginase 2 preserves visual function after optic
693 nerve crush. *Cell Death Dis* **14**, 661 (2023).
694 39. G. T. Prusky, N. M. Alam, S. Beekman, R. M. Douglas, Rapid quantification of adult
695 and developing mouse spatial vision using a virtual optomotor system. *Invest*
696 *Ophthalmol Vis Sci* **45**, 4611-4616 (2004).
697 40. R. M. Douglas, N. M. Alam, B. D. Silver, T. J. McGill, W. W. Tschetter, G. T. Prusky,
698 Independent visual threshold measurements in the two eyes of freely moving rats
699 and mice using a virtual-reality optokinetic system. *Vis Neurosci* **22**, 677-684 (2005).

41. A. Y. Fouda, Z. Xu, J. Suwanpradid, M. Rojas, E. Shosha, T. Lemtalsi, C. Patel, J. Xing, S. A. Zaidi, W. Zhi, B. K. Stansfield, P. N. Cheng, S. P. Narayanan, R. W. Caldwell, R. B. Caldwell, Targeting proliferative retinopathy: Arginase 1 limits vitreoretinal neovascularization and promotes angiogenic repair. *Cell Death Dis* **13**, 745 (2022).

Figure 1

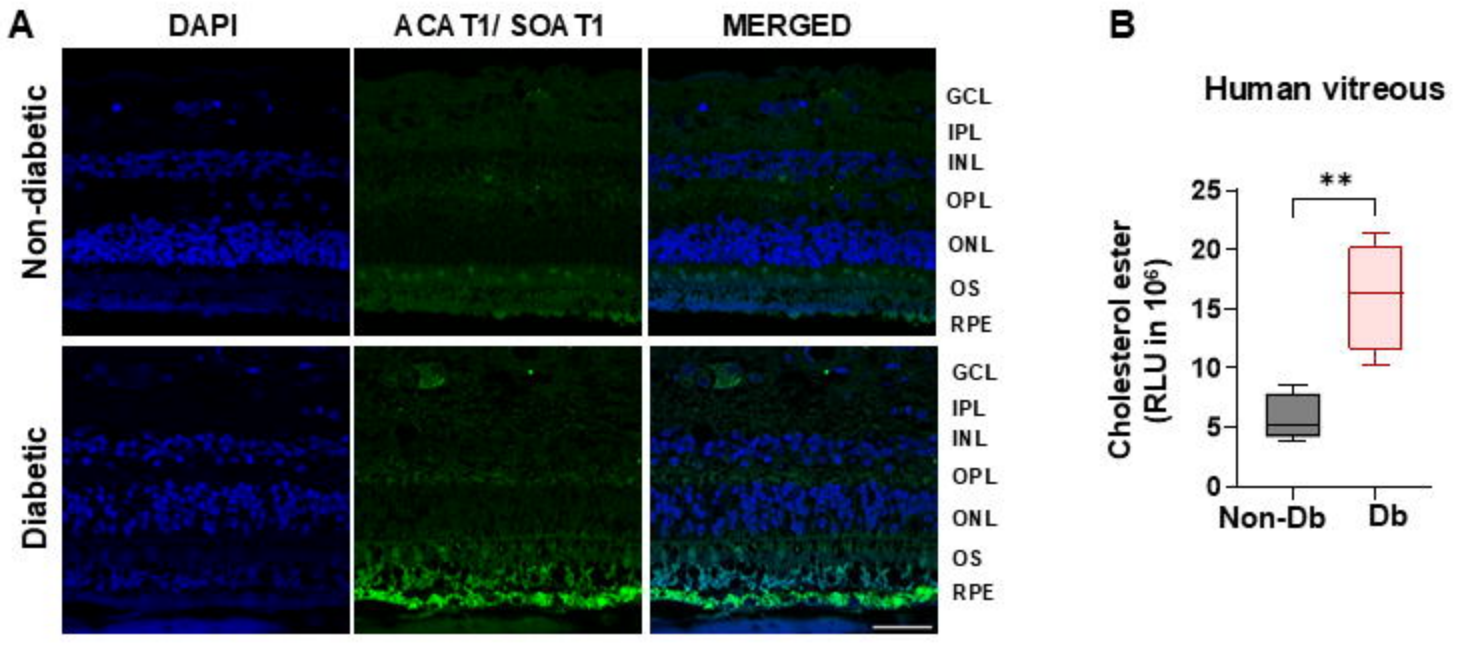

Figure 1. ACAT1/SOAT1 expression and activity are upregulated in retina and vitrectomy samples from patients with diabetic retinopathy (DR).

A. Immunolabeling of retina sections from human donors with DR showed increased ACAT1/SOAT1 immunoreactivity in the photoreceptor outer segments (OS) and retinal pigment epithelial (RPE) cells, as compared with non-diabetic control donors. Donor sample information is provided in Supplementary Table 1. Scale bar = 50 µm. n=3. **B.** Vitrectomy tissues collected from patients with PDR showed an increased level of CE, as measured by ELISA. Donor sample information is provided in Supplementary Table 2. Data are presented as mean ± SEM. n=4-5. **$p<0.01$.

Figure 2

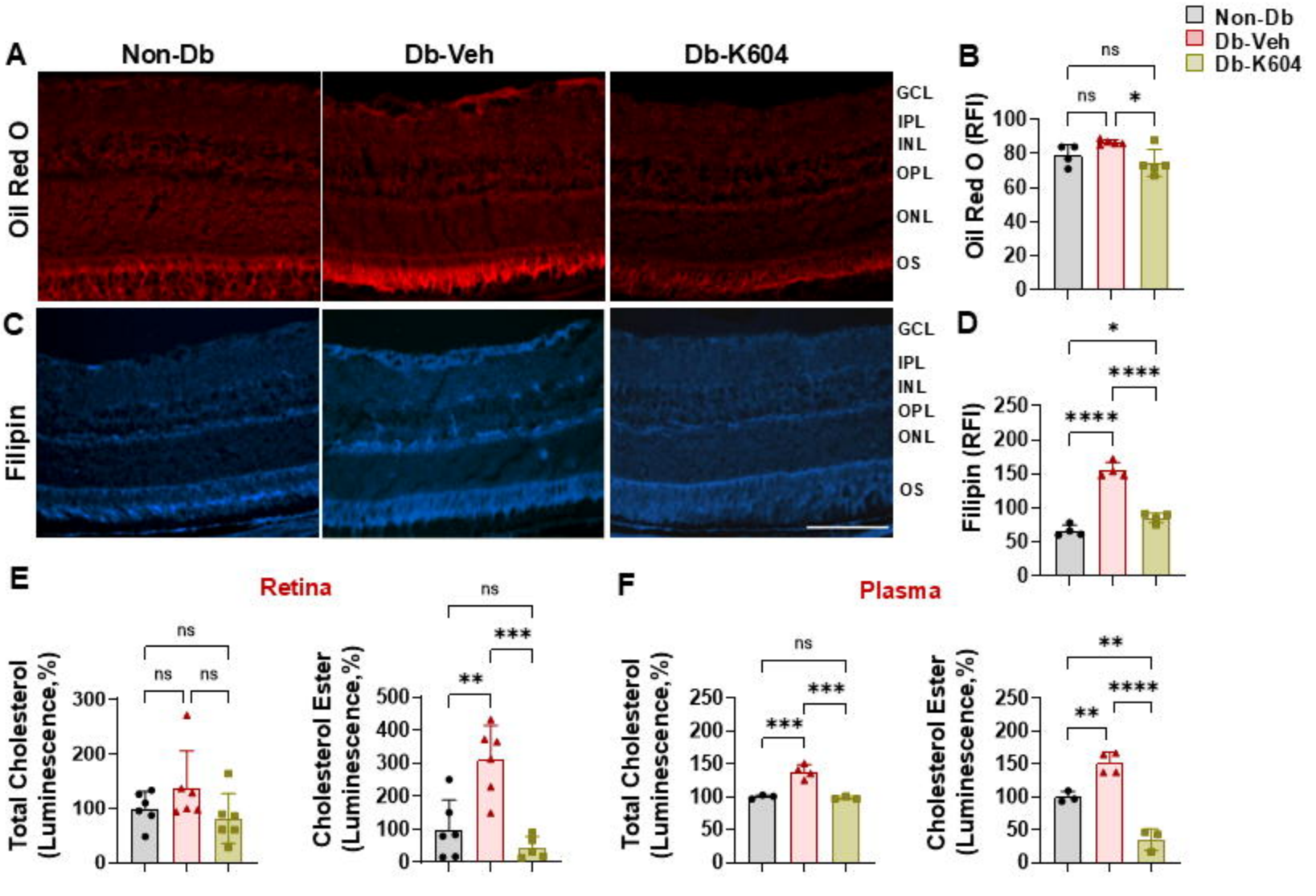

Figure 2. Inhibition of ACAT1/SOAT1 prevents diabetes-induced CE formation in Ins2^{Akita} mice. Ten-week old male diabetic Ins2^{Akita} mice were treated with PBS as vehicle or ACAT1/SOAT1 inhibitor, K604 (10mg/Kg, i.p.), every 2 days for 2 weeks. After 2 weeks of treatment eyeballs and retinas were collected. **A-B.** Oil red O staining of frozen sections shows mild reactivity in the ganglion cell layer (GCL) and photoreceptor outer segments (OS) of the Ins2^{Akita} diabetic retina. Treatment with the ACAT1/SOAT1 inhibitor, K604, reduced this activity. Data are presented as mean ± SEM. n=4-5. *p<0.05, ns: not significant. **C-D.** Detection of CE by filipin labeling of frozen retina sections shows prominent increases in CE formation in the ganglion cell (GCL), outer plexiform (OPL) and photoreceptor outer segment (OS) layers of the Ins2^{Akita} diabetic retina. Treatment with K604 prevented the CE increase. Data are presented as mean ± SEM. Scale bar = 40 µm. n=4. *p<0.05, ****p<0.0001. **E-F.** Total cholesterol and CE levels were measured in retinas and plasma from non-diabetic control mice, Ins2^{Akita} diabetic mice, and K604-treated Ins2^{Akita} diabetic mice. This analysis showed upregulation of total cholesterol in plasma of the Ins2^{Akita} mice but not in retina. However, CE was increased in both retina and plasma of the Ins2^{Akita} mice. K604 treatment reduced retinal CE formation as well as preventing the increases in both cholesterol and CE in plasma. Data are presented as mean ± SEM. n=4-6. **p<0.01, ***p<0.001, ****p<0.0001, ns: not significant.

Figure 3

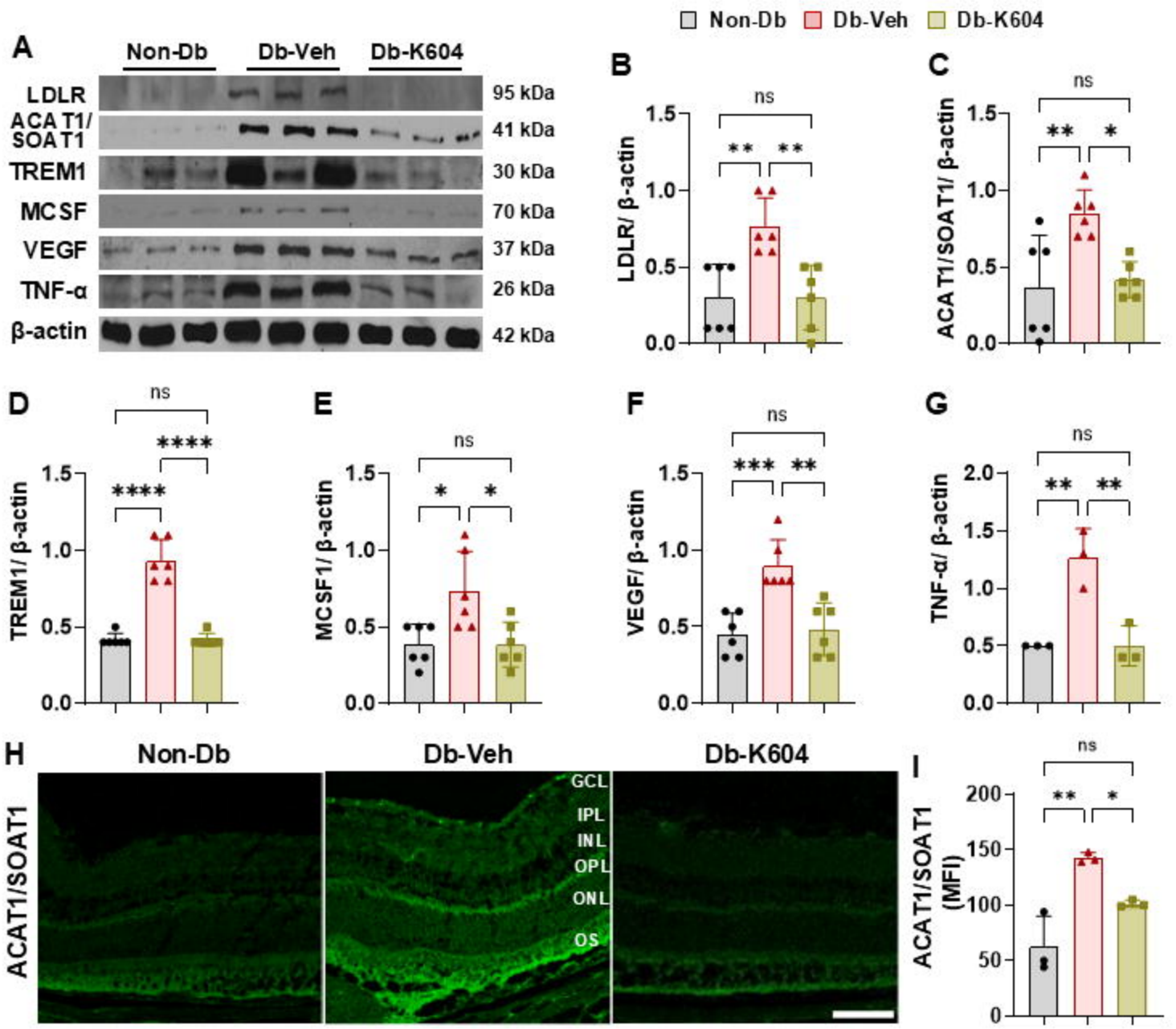

Figure 3. Inhibition of ACAT1/SOAT1 prevents diabetes-induced increases in expression of inflammatory mediators and ACAT1/SOAT1 in Ins2^{Akita} mice. A. Western blot analysis of retinas from 12-week diabetic Ins2^{Akita} mice showed marked increases in **B.** LDLR, **C.** ACAT1/SOAT1, **D.** TREM1, **E.** MCSF, **F.** VEGF, and **G.** TNF-α as compared with the WT non-diabetic controls. These increases were normalized by the treatment with K604 (10mg/Kg, ip) every two days from 10 to 12 weeks. Data are presented as mean ± SEM. n=3-6. *p<0.05, ns: not significant. **H-I**. Increased immunoreactivity for ACAT1/SOAT1 was detected in retinal frozen sections from Ins2^{Akita} diabetic mice, especially in the RGC, OPL, and OS layers. The ACAT1 immunoreactivity was significantly reduced in retinas of Ins2^{Akita} diabetic mice treated with K604. Data are presented as mean ± SEM. n=3. Scale bar = 25 μm. *p<0.05, **p<0.01, ns: not significant

Figure 4

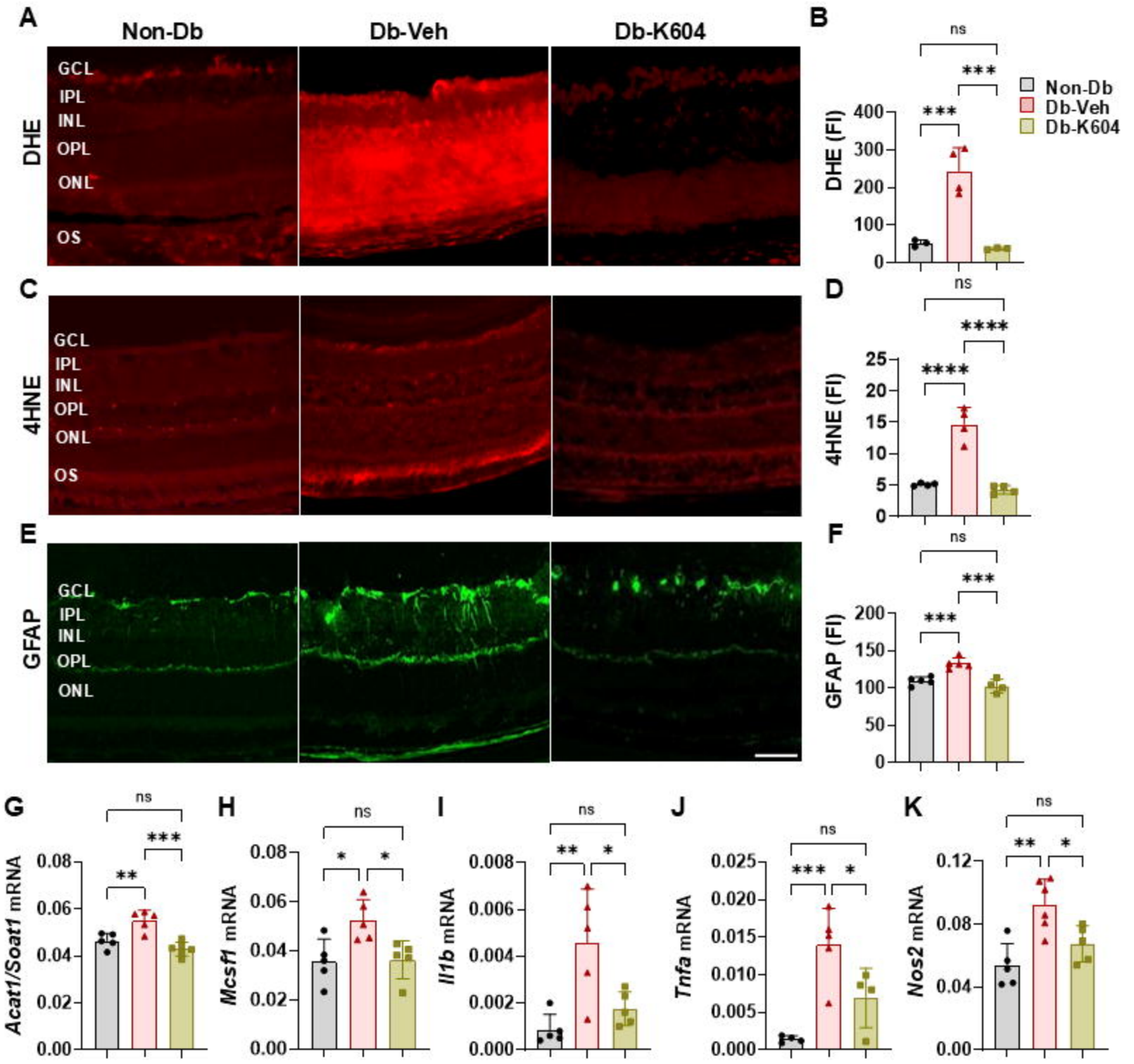

Figure 4. Inhibition of ACAT1/SOAT1 ameliorates the diabetes-induced increases in oxidative stress, gliosis, and expression of inflammatory mediators in Ins2^{Akita} mice. A-B. DHE imaging showed upregulation of superoxide formation in frozen sections from Ins2^{Akita} diabetic mice. This effect was blocked by the K604 treatment. Data are presented as mean ± SEM. n=4. ***p<0.001, ns: not significant. **C-D.** Immunofluorescent labeling of frozen retina sections with 4-hydroxynonenal (4-HNE) and fluorescence intensity quantification showed increased 4-HNE levels in the ganglion cell layer (GCL), outer plexiform layer (OPL) and photoreceptor outer segments (OS) of the Ins2^{Akita} mice. K604 treatment blocked this effect. Data are presented as mean ± SEM. n=4. ****p<0.0001, ns: not significant. **E-F.** Immunolabeling of retina cross-sections showed increased GFAP immunoreactivity in Müller cells of the Ins2^{Akita} mice, which was blocked in the K604 treated mice. Data are presented as mean ± SEM. Scale bar=30 µm. n=4. ***p<0.001, ns: not significant. **G-K.** Quantitative RT-PCR showed upregulation of *Acat1/Soat1*, along with proinflammatory mediators – *Mcsf1, Il1b, Tnfa*, and *Nos2* in Ins2^{Akita} diabetic mouse retinas, compared to non-diabetic controls. K604 treatment significantly inhibited these increases. n=4-6. Data are presented as mean ± SEM. *p<0.05, **p<0.01, ***p<0.00, ns: not significant.

Figure 5

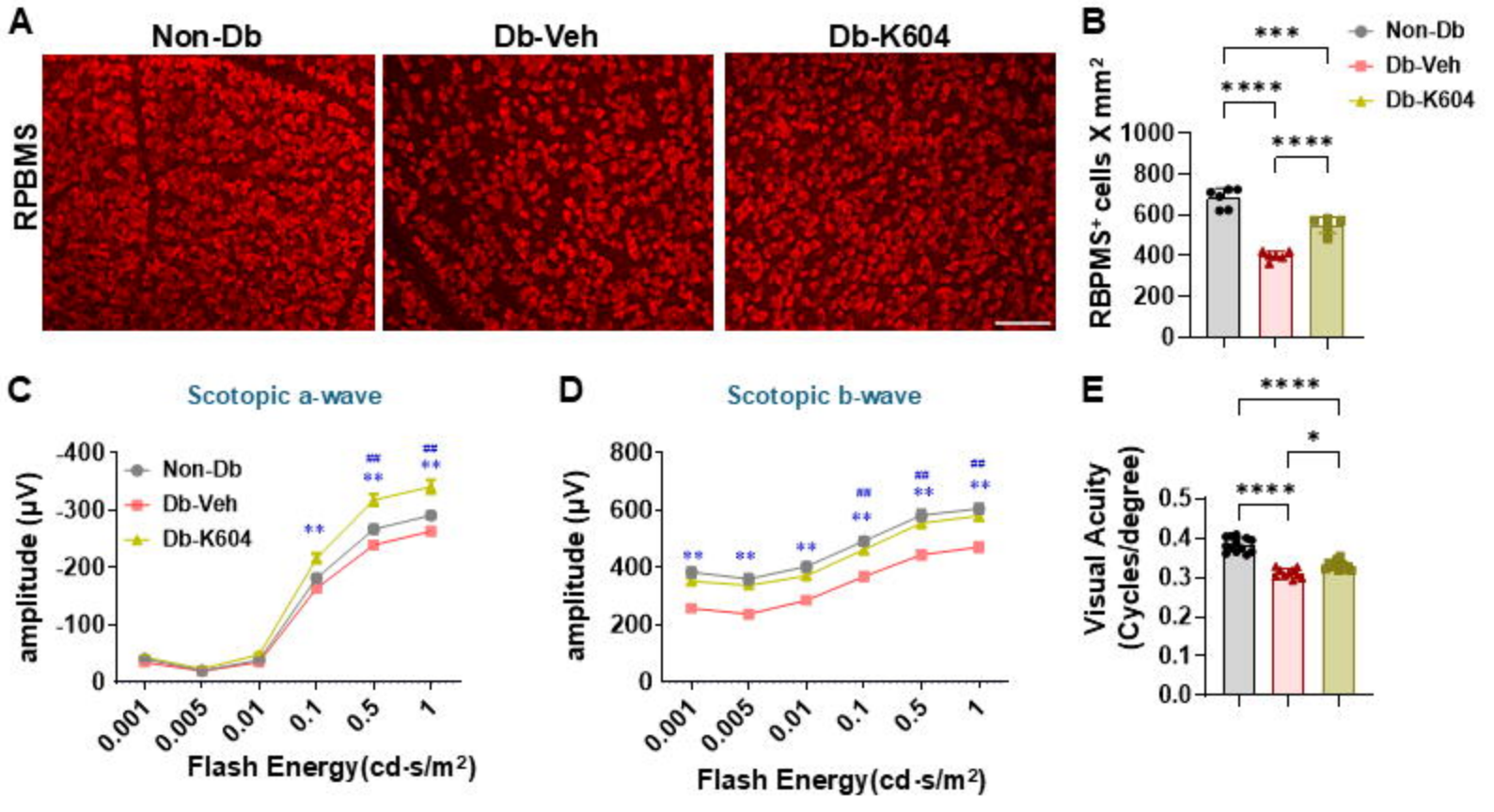

Figure 5. Inhibition of ACAT1/SOAT1 limits retinal ganglion cell loss and improves visual function in Ins2^{Akita} diabetic mice. Ten-week-old male diabetic Ins2^{Akita} mice were treated with ACAT1/SOAT1 inhibitor, K604 (10 mg/Kg, ip), every 2 days for 2 weeks. After 2 weeks, retinas were collected for analysis **A-B.** Confocal imaging of retinal flatmounts labeled with the neuronal marker, RBPMS and quantification showed a significant decrease in RPBMS positive retinal ganglion cells in vehicle-treated Ins2^{Akita} diabetic retinas compared to the non-diabetic control retinas. This retinal ganglion cell loss was markedly reduced by the K604 treatment. Data are presented as mean ± SEM. Scale bar=40 μm. n=5-6. ***p<0.001, ****p<0.0001. **C-D**. Retinal function was measured by electroretinography (ERG). Both scotopic a-wave and scotopic b-wave were improved in K604-treated Ins2^{Akita} diabetic mice as compared with the vehicle treated diabetic mice. Data are presented as mean ± SEM, n=12–26, **p<0.01 non-diabetic versus vehicle-treated diabetic mice; $^{\#\#}$p<0.01 vehicle-treated diabetic versus K604-treated diabetic mice. **E**. Measurement of visual acuity by optoMotry responses (OMR) showed a marked improvement in the K604-treated diabetic mice as compared with the vehicle-treated diabetic mice. Data are presented as mean ± SEM. n=10-13. *p<0.05, ****p<0.0001.

Figure 6

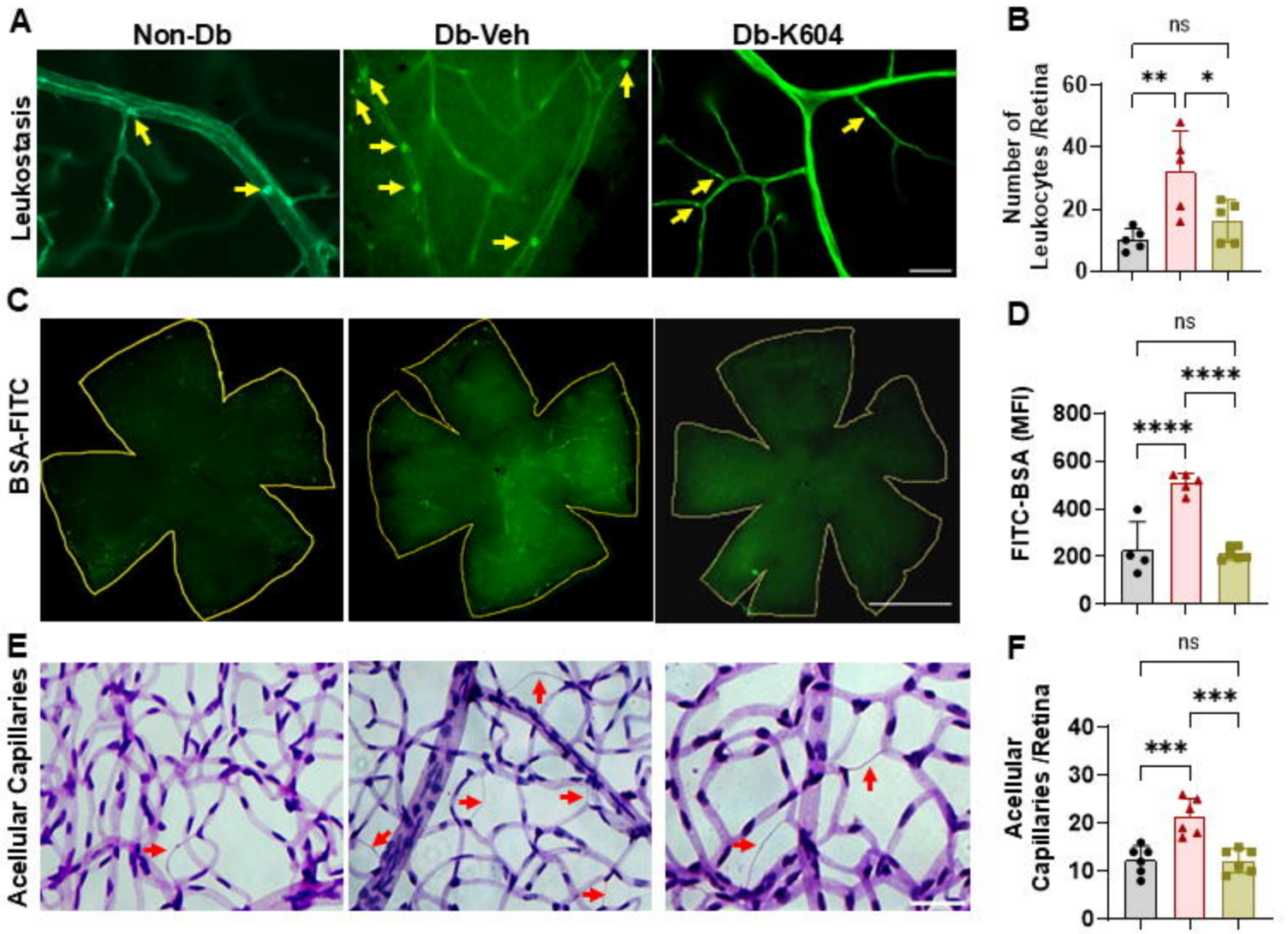

Figure 6. Inhibition of ACAT1/SOAT1 prevents diabetes-induced microvascular abnormalities (leukostasis, vascular permeability and acellular capillaries) in Ins2^{Akita} diabetic mice. Ten week old male diabetic Ins2^{Akita} mice were treated with ACAT1/SOAT1 inhibitor, K604 (10 mg/Kg, ip), every 2 days for 2 weeks. After the 2 weeks treatment, retinas were collected for analysis. **A-B.** Quantitative analysis shows diabetes-induced increases in leukocyte adhesion in Ins2^{Akita} retinal vessels, which were significantly prevented by K604 treatment as compared with vehicle. Data are presented as mean ± SEM. n=5-6. Scale bar=50 µm. *p<0.05, **p<0.01, ns: not significant. **C-D**. Vascular leakage was visualized and quantified by measuring the fluorescence intensity of FITC-conjugated BSA. K604 treatment significantly prevented vascular leakage in Ins2^{Akita} mice as compared with vehicle controls. Data are presented as mean ± SEM. n=5-6. Scale bar=300 µm. ****p<0.0001, ns: not significant. **E**. K604 treatment significantly prevented diabetes-induced increases in acellular capillary formation as compared with the vehicle controls. Data are presented as mean ± SEM. n=6. Scale bar=40 µm. ***=p<0.001, ns=not significant.

Figure 7

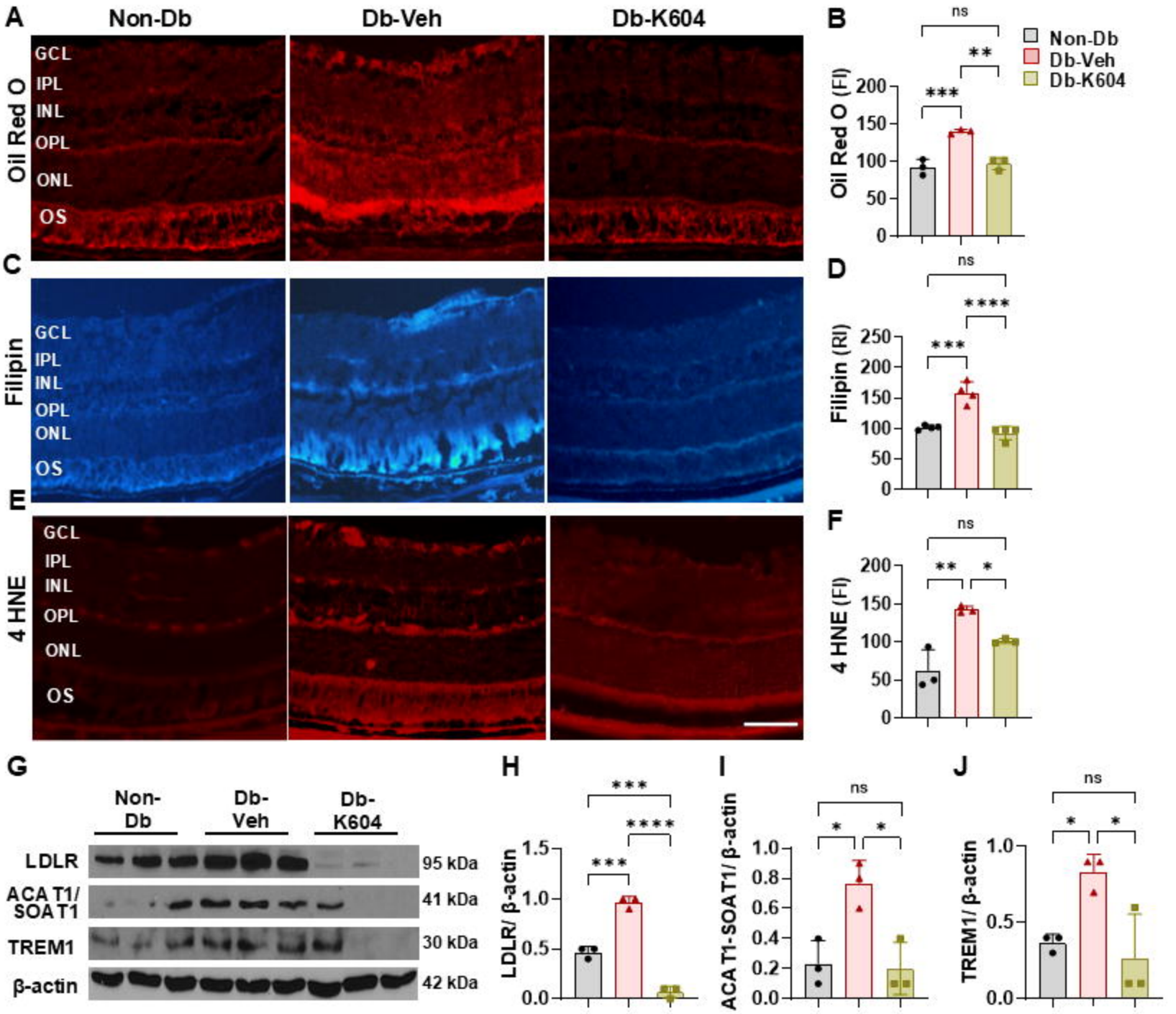

Figure 7. Inhibition of ACAT1/SOAT1 limits the progression of later stage DR-induced lipid/cholesterol accumulation and inflammation. Eight-months-old male $Ins2^{Akita}$ diabetic mice were treated with ACAT1/SOAT1 inhibitor, K604 (10 mg/Kg, ip), every 2 days for 2 months. After the 2 months treatment, retinas were collected for analysis. Oil red O staining (**A,B**), filipin staining (**C,D**) and 4HNE staining (**E,F**) of frozen sections shows a strong reaction in areas of the ganglion cell layer (GCL) and photoreceptor outer segments (OS) of the DR retina, indicating lipid accumulation, CE formation, and oxidative stress, respectively. Treatment with the ACAT1/SOAT1 inhibitor, K604, significantly blocked these effects. Data are presented as mean ± SEM. Scale bar=25 μm. n=3-4. *p<0.05, **p<0.01, ***p<0.001, ****p<0.0001, ns=not significant. **G-J.** Western blot analysis of retinal samples from the $Ins2^{Akita}$ diabetic mice showed marked increases in LDLR, ACAT1/SOAT1, and TREM1, as compared with the WT non-diabetic controls. These increases were normalized by treatment with K604. Data are presented as mean ± SEM. n=3. *p<0.05, ***p<0.001, ****p<0.0001, ns=not significant.

Figure 8.

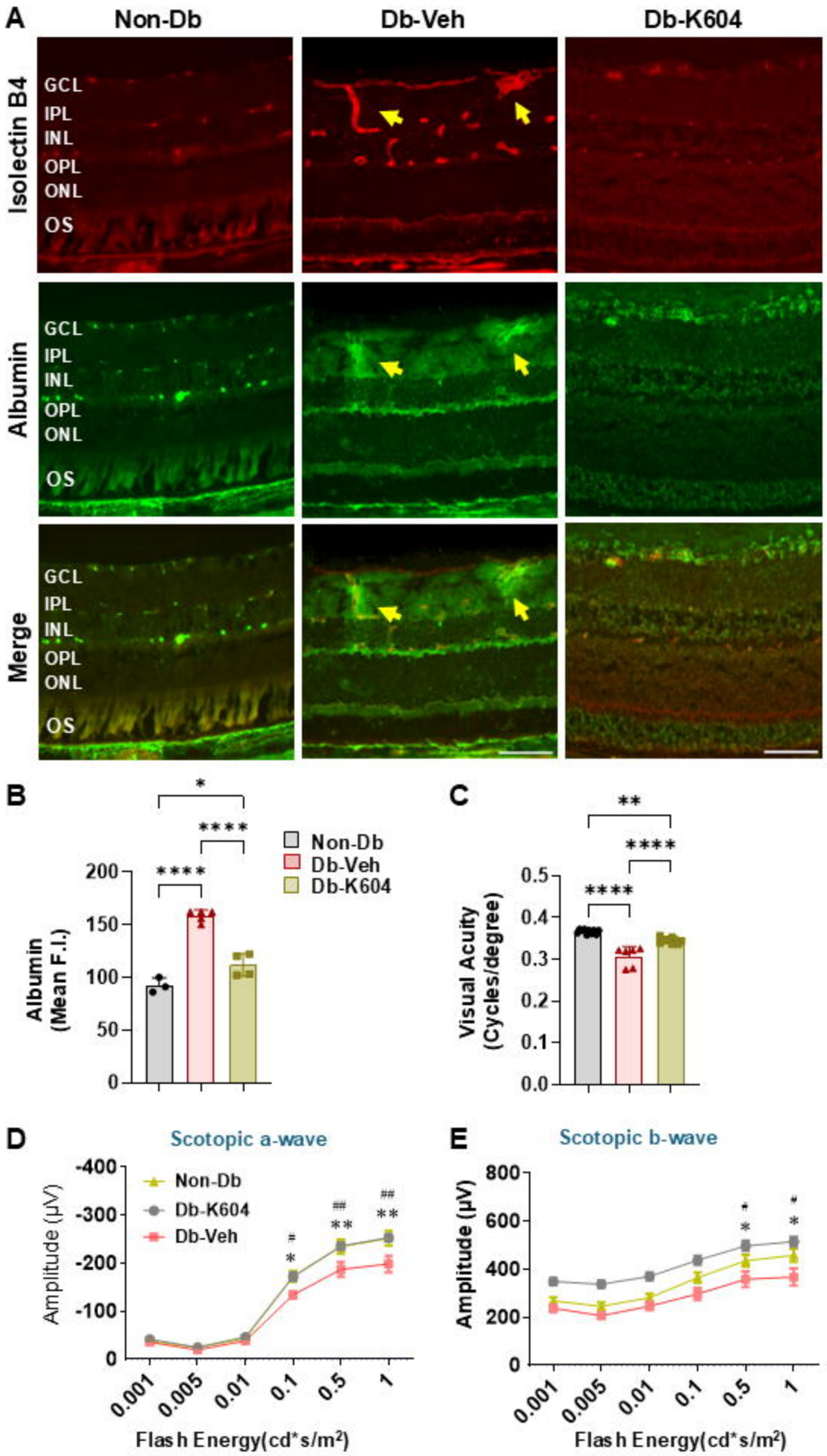

Figure 8. ACAT1/SOAT1 inhibitor treatment limits vascular leakage and preserves visual function in later stage DR. Eight-months old male $Ins2^{Akita}$ diabetic mice were treated with ACAT1/SOAT1 inhibitor, K604 (10 mg/Kg, ip), every 2 days for 2 months. After 2 months, retinas were collected for analysis. **A-B.** Albumin staining of retina sections showed a strong reaction in areas of Isolectin B4-positive blood vessels in the diabetic retina, indicating vascular leakage. Treatment with ACAT1/SOAT1 inhibitor, K604, significantly blocked this effect. Data are presented as mean ± SEM. n=3-4. Scale bar=25 μm. *p<0.05; ****p<0.0001. **C.** Measurement of visual acuity by optoMotry responses (OMR) showed a significant impairment in the vehicle-treated diabetic $Ins2^{Akita}$ mice that was significantly blunted in the K604-treated diabetic mice. Data are presented as mean ± SEM. n=6-10. **p<0.01, ****p<0.0001. **D-E.** Electroretinography (ERG) showed improvement in both scotopic a-wave and scotopic b-wave in K604-treated diabetic mice as compared with the vehicle treated diabetic mice. Data are presented as mean ± SEM. n=6-10. *p<0.05, **p<0.01 non-diabetic versus vehicle-treated diabetic mice; #p<0.05, ##p<0.01 vehicle-treated diabetic versus K604-treated diabetic mice.